



The University of Bradford Institutional Repository

<http://bradscholars.brad.ac.uk>

This work is made available online in accordance with publisher policies. Please refer to the repository record for this item and our Policy Document available from the repository home page for further information.

To see the final version of this work please visit the publisher's website. Available access to the published online version may require a subscription.

Link to original published version:

<https://www.concrete.org/publications/internationalconcreteabstractsportal.aspx?m=details&ID=19944>

Citation: Yang KH and Ashour AF (2008) Mechanism analysis for concrete breakout capacity of single anchors in tension. ACI Structural Journal, 105 (5): 609-616.

Copyright statement: © 2008 ACI. Reproduced in accordance with the publisher's self-archiving policy.



MECHANISM ANALYSIS FOR CONCRETE BREAKOUT CAPACITY OF SINGLE ANCHORS IN TENSION

Keun-Hyeok Yang^a and Ashraf F. Ashour^b

^a *Corresponding author, Department of Architectural Engineering, Mokpo National University, Mokpo, Jeonnam, South Korea.*

^b *EDT1, School of Engineering, Design and Technology, University of Bradford, Bradford, BD7 1DP, UK.*

Biography: K. H. Yang is an assistant professor at Mokpo National University, South Korea. He received his MSc and PhD degrees from Chungang University, Korea. His research interests include ductility, strengthening, plasticity and shear of reinforced concrete structures.

A.F.Ashour is a senior lecturer at the University of Bradford, UK. He obtained his BSc and MSc degrees from Mansoura University, Egypt and his PhD from Cambridge University, UK. His research interests include shear, plasticity, repair, strengthening and optimisation of reinforced concrete and masonry structures.

ABSTRACT

A numerical technique based on the theory of plasticity is developed to predict an optimum failure surface generatrix and concrete breakout capacity of single anchors away from edges under tensile loads. Concrete is regarded as a rigid perfectly plastic material obeying a modified Coulomb failure criteria with effective compressive and tensile strengths. The failure mode is idealized as an

assemblage of two rigid blocks separated by failure surfaces of displacement discontinuity. Minimisation of the collapse load predicted by the energy equation produces the optimum shape of the failure surface generatrix. A simplified solution is also developed by approximating the failure surface as two straight lines.

The effect of different parameters on the concrete breakout capacity of anchors is reviewed using the developed mechanism analysis, ACI 318-05, and test results of 501 cast-in-place and 442 post-installed anchor specimens. The shape of failure surface and concrete breakout capacity of anchors predicted by the mechanism analysis are significantly affected by the ratio between effective tensile and compressive strengths of concrete. For anchors installed in concrete having a low ratio between effective tensile and compressive strengths, a much larger horizontal extent of failure planes in concrete surface is predicted by the mechanism analysis than recommended by ACI 318-05, similar to test results. Experimental concrete breakout capacity of anchors is closer to the prediction obtained from the mechanism analysis than ACI 318-05. ACI 318-05 provisions for anchors sharply underestimate the breakout capacity of cast-in-place and post-installed anchors having effective embedment depths exceeding 200 mm and 80 mm, respectively, installed in concrete of compressive strength larger than 50 MPa.

Keywords: anchors, concrete breakout capacity, failure surface generatrix, upper-bound theorem, ACI 318-05.

INTRODUCTION

Anchors for load transfer between concrete and steel members enable flexibility in the design of concrete structures. Anchors can be classified into two groups: 1) cast-in-place anchors such as headed studs or headed bolts and 2) post-installed anchors such as expansion anchors, bonded (adhesive) anchors, and undercut anchors¹⁻³. Depending on the concrete strength, the embedment

depth and steel yield strength of the anchor, and the edge distance, five failure modes² of anchors subjected to tension can be identified as: steel yielding (or rupture), concrete bursting, anchor pull-out, concrete splitting and concrete breakout failure. Among these failure modes, concrete breakout failure is the most common and brittle. Therefore, correct estimation of the concrete breakout capacity of anchors under tensile loads would permit the nominal anchor strength to be controlled by ductile yielding.

Fuchs et al.³ showed that concrete breakout failure can be reasonably predicted by the concrete capacity design (CCD) method on which design provisions for anchoring system of ACI 318-05² are based. However, Cannon⁴ pointed out that the CCD approach for practical design is limited to anchors having an effective embedment depth less than 250 mm since it was developed from limited anchor size and embedment depth. Primavera et al.⁵ concluded that concrete breakout capacity of cast-in-place anchors in concrete of compressive strength above 50 MPa was highly overestimated by the CCD method and the angle of failure planes to the concrete member longitudinal axis ranged from 21° to 28° unlike the assumption of ACI 318-05. Therefore, the ACI 318-05 provisions for anchors need to be reviewed for high concrete strength and large embedment depths. In addition, a mechanism analysis for concrete breakout failure of anchors is developed to complement the CCD method based on an equilibrium approach and calibrated against limited test results.

This study presents a numerical technique using the upper-bound theorem of the theory of plasticity to predict the optimum geometry of the failure surface and hence obtain an upper bound on the concrete breakout capacity of single anchors under tensile loads. The influence of concrete tensile strength on the failure surface generatrix and concrete breakout capacity of anchors is examined. The effect of different parameters on the concrete breakout capacity of anchors is also reviewed using the mechanism analysis, ACI 318-05, and a database compiled from tension tests on 501 cast-in-place and 442 post-installed anchors.

SIGNIFICANCE OF RESEARCH

The ACI 318-05 provisions for concrete breakout capacity of single anchors under tensile loads are applicable for limited ranges of concrete compressive strength and effective embedment depth as they are based on the empirical CCD method. The horizontal extent of the assumed breakout body is always fixed. The mechanism analysis developed in the present study shows that the shape of the failure surface and the concrete breakout capacity of anchors loaded to failure in tension are significantly dependent on the ratio between effective tensile and compressive strengths of concrete.

CONCRETE BREAKOUT STRENGTH OF ANCHORS IN ACI 318-05

The idealized failure mode of concrete breakout of single anchors under tensile loads adopted in ACI 318-05 is shown in Fig. 1. Although a cone shaped concrete block having nonlinear failure surface generatrix was commonly observed at failure^{1, 3, 5, 6}, ACI 318-05 idealized the failed block as a pyramid shape having an inclination of approximately 35° measured from the failure surface to a plane perpendicular to anchor axis. As a result, the horizontal extent of failure planes in concrete surface is taken as three times the effective embedment depth h_{ef} of anchors and the distance between failure planes formed in concrete surface and anchor center is $1.5h_{ef}$ as shown in Fig. 1.

ACI 318-05 specifies the concrete breakout capacity N_{cb} of single anchors under tensile loads in a region of a concrete member where analysis indicates no cracking and no edge effect as follows:

$$N_{cb} = k_c \sqrt{f'_c} h_{ef}^{1.5} \quad (1)$$

where $k_c \equiv 12.5$ (30 for concrete strength in psi) for cast-in-place anchors, and 9.8 (23.8 for concrete strength in psi) for post-installed anchors, and f'_c = concrete compressive strength.

The practical application of Eq. (1) is limited by concrete strength, and size and embedment depth of anchors as it is based on the CCD method that was calibrated against a limited range of test data;

in sum, f'_c used in Eq. (1) should not exceed 70 MPa (10150 psi) for cast-in-place anchors and 55 MPa (7975 psi) for post-installed anchors, and embedment depth of anchors should be below 635 mm (25 in.). In addition, for cast-in-place headed studs and bolts with embedment depth between 280 mm (11 in.) and 635 mm (25 in.), the upper limit $N_{cb,max}$ of concrete breakout capacity of anchors in uncracked concrete is optionally given as follows:

$$N_{cb,max} = 4.87\sqrt{f'_c}h_{ef}^{5/3} \quad (2)$$

The value obtained from Eq. (2) exceeds that calculated from Eq. (1) for anchors having effective embedment depth exceeding about 285 mm (11 in.).

MECHANISM ANALYSIS

Failure mechanism

Fig 2 shows an axisymmetric surface of concrete breakout failure of single anchors under tension observed in widespread concrete breakout specimens^{1, 3, 5, 6}. At failure, a concrete member can be idealized as two rigid blocks separated by failure surface, one of which vertically moves relative to the longitudinal axis of the other fixed rigid block by an amount δ . The separated block with the anchor has a truncated cone shape having a nonlinear generatrix of failure surfaces. Therefore, the horizontal extent d_1 of failure plane at concrete surface and the angle α between the relative displacement δ and failure surface are variables as presented in Fig. 2. For the idealized failure mechanism, the strain ε_{zz} in the circumferential direction is zero; hence the generatrix can be considered as a yield line, representing the zones of intense concrete separation, in a state of plane strain.

Modelling of concrete

Concrete is regarded as a rigid perfectly plastic material obeying a modified Coulomb failure criteria with effective compressive and tensile strengths^{7,8} as given in Fig. 3 for plane strain case. Nielsen⁸ showed that in many respects concrete can be modelled as a modified Coulomb material. The effective compressive f_c^* and tensile f_t^* strengths of concrete can be expressed as below⁸:

$$f_c^* = \nu_c f_c' \quad (3)$$

$$f_t^* = \nu_t f_t' \quad (4)$$

where ν_c and ν_t = effectiveness factors for measured compressive f_c' and tensile f_t' strengths of concrete, respectively.

Upper bound solution

To evaluate the geometry of the failure surface generatrix, the failure depth is divided into n segments as shown in Fig 2. For each layer, the vertical coordinate y_i is fixed, dependent on the number of segments and the horizontal coordinate x_i is varied and would be obtained after minimising the collapse load according to the plasticity theory. The normality condition of a modified Coulomb material in the state of plane strain requires that the angle between the relative displacement and yield line should be larger than a friction angle φ at failure plane as proved by

Nielsen⁸, namely, $\alpha_i = \tan^{-1} \frac{x_i - x_{i-1}}{y_i - y_{i-1}} \geq \varphi$. Nielsen⁸ and Bræstrup⁹ also showed that the friction

angle φ of concrete having a modified Coulomb yield criteria can be reasonably assumed as 37° .

The upper bound analysis uses the energy principle to calculate the load capacity for the kinematically admissible failure mechanism. From Fig. 2, the external work W_E at failure is

$$W_E = N_{cb} \delta \quad (5)$$

The internal energy $(W_I)_i$ dissipated in each concrete layer i would be estimated as below:

$$(W_I)_i = (W_A)_i A_i \quad (6)$$

where $(W_A)_i$ and A_i = dissipated energy per unit area and failure surface area of concrete layer i , respectively. The dissipation per unit area is^{7,8}

$$(W_A)_i = \frac{1}{2} f_c^* \delta [l - m \sin \alpha_i] \quad (7)$$

where $l = 1 - 2\mu \frac{\sin \varphi}{1 - \sin \varphi}$, $m = 1 - 2\mu \frac{1}{1 - \sin \varphi}$, and $\mu = \frac{f_t^*}{f_c^*}$ = ratio between effective tensile and compressive strengths of concrete. Failure surface area A_i of layer i having a truncated cone shape is found by integration over the layer depth as follows:

$$\begin{aligned} A_i &= \int_{y_{i-1}}^{y_i} 2\pi r(y_i) \frac{dy}{\cos \alpha_i} = \frac{2\pi}{\cos \alpha_i} \int_{y_{i-1}}^{y_i} [x_{i-1} + (y - y_{i-1}) \tan \alpha_i] dy \\ &= \frac{\pi (y_i - y_{i-1})}{\cos \alpha_i} [(y_i - y_{i-1}) \tan \alpha_i + 2x_{i-1}] \end{aligned} \quad (8)$$

Equating the total internal energy dissipated in concrete to the external work done, the concrete breakout capacity N_{cb} of single anchor can be derived in the following form:

$$N_{cb} = \frac{\pi}{2} f_c^* \sum_{i=1}^n [l - m \sin \alpha_i] \frac{(y_i - y_{i-1}) [(y_i - y_{i-1}) \tan \alpha_i + 2x_{i-1}]}{\cos \alpha_i} \quad (9)$$

The concrete breakout capacity N_{cb} of single anchor is implicitly expressed as a function of the geometry of the failure surface generatrix as proposed by Eq. (9). According to the upper-bound theorem, the collapse occurs at the least strength. The minimum value of concrete breakout capacity can be obtained by varying the horizontal coordinate x_i of each layer since the vertical coordinate y_i of each layer is known as shown in Fig. 2. It is noted that the angle α_i of each layer should be larger than the friction angle φ as explained above. The process of adjusting the horizontal coordinate x_i of each layer to evaluate the optimum geometry of failure surface generatrix is achieved by reliable numerical optimization procedures programmed in Matlab software¹⁰.

Failure surface generatrices

Examples of optimum failure surface generatrices for different d_B/h_{ef} , where d_B = anchor head diameter, obtained from the above mechanism analysis are plotted in Fig. 4: Fig. 4 (a) for the ratio between effective tensile and compressive strengths μ of 0.01 and Fig. 4 (b) for μ of 0.0025. On the same figure, the failure surface generatrix specified in ACI 318-05 is also presented. The shape of failure surface generatrices predicted by the mechanism analysis is greatly influenced by μ , agreeing with test results recorded by Primavera et al.⁵. For anchors installed into concrete having μ of 0.01, the horizontal extent of failure planes in concrete surface obtained from the mechanism analysis is similar to that of ACI 318-05. However, much larger extended failure planes for anchors installed into concrete having μ of 0.0025 are predicted by the mechanism analysis than ACI 318-05. In addition, it was observed by Primavera et al.⁵ that the horizontal extent of failure planes specified in ACI 318-05 was unconservative for anchors installed in high-strength concrete above 50 MPa (7250 psi). This would have a significant influence on predicting concrete breakout capacity of a group of anchors or close to edge anchors installed in high strength concrete. In particular, the maximum spacing between anchors in a group or a critical edge distance for anchors should be designed considering reliable failure surface generatrices, though ACI 318-05 specifies a constant shape of failure surface, regardless of anchor type and concrete compressive strength. Hence, a simple, rational procedure to evaluate the failure surface generatrices is developed below.

Simplified solution

The above iterative procedure to find the optimum failure surface generatrix and the corresponding concrete breakout capacity of anchors is not suitable for practical design; therefore a simplified analysis is developed and presented below. The optimum failure surface generatrices shown in Fig.

4 can be simplified as two straight lines as given in Fig. 5. From Eq. (9), concrete breakout capacity of anchors for cone-shaped failure surface having two straight generatrices can be produced as follows:

$$N_{cb} = \frac{\pi}{2} f_c^* \left[\frac{h_0 (d_B + h_0 \tan \varphi)}{\cos \varphi} (1 - \sin \varphi) + \frac{(h_{ef} - h_0) \{ (h_{ef} - h_0) \tan \alpha + d_B + 2h_0 \tan \varphi \}}{\cos \alpha} (l - m \sin \alpha) \right] \quad (10)$$

where h_0 = depth of the bottom failure zone as represented in Fig. 5. Therefore, the first and second terms in the right hand side of Eq. (10) give the dissipated energies in zone AB having angle φ and zone BC having angle α , respectively, as shown in Fig. 5. Assuming that the angle φ is equal to α , the concrete breakout capacity of anchors as given by Eq. (10) is a function of h_0 and α . Thus the lowest upper-bound solution can be obtained by letting $\partial N / \partial h_0 = 0$ and $\partial N / \partial \alpha = 0$. When $\partial N / \partial h_0 = 0$, h_0 can be obtained as follows:

$$h_0 = - \frac{d_B \{ \cos \alpha (\sin \varphi - 1) + \cos \varphi (l - m \sin \alpha) \} + 2h_{ef} \cos \varphi \{ l (\tan \alpha - \tan \varphi) + m \sin \alpha (\tan \varphi - \tan \alpha) \}}{2 [\tan \varphi \cos \alpha (\sin \varphi - 1) - \cos \varphi \tan \alpha (l - m \sin \alpha) + 2 \cos \varphi \tan \varphi (l - m \sin \alpha)]} \quad (11)$$

As $\partial N / \partial \alpha = 0$, the expression below to find α can be driven.

$$\left[\begin{array}{l} -m (h_f - h_0) \{ (h_f - h_0) \tan \alpha + d_B + 2h_0 \tan \varphi \} + \frac{(l - m \sin \alpha) (h_f - h_0)^2 (1 + \tan^2 \alpha)}{\cos \alpha} \\ + \frac{(l - m \sin \alpha) (h_f - h_0) \{ (h_f - h_0) \tan \alpha + d_B + 2h_0 \tan \varphi \} \sin \alpha}{\cos^2 \alpha} \end{array} \right] = 0 \quad (12)$$

Substituting Eq. (11) into Eq. (12) and then using numerical techniques for solving non-linear equations, the angle α would be obtained. Fig. 6 shows the angle α estimated using the bi-section method and the corresponding normalized depth h_0 / h_{ef} of failure zone for different parameters.

The angle α is significantly affected by μ but independent on the normalized anchor head diameter d_B / h_{ef} and h_{ef} , showing that the smaller the μ , the larger the α . If concrete tensile

strength is ignored ($f_t^* = 0$), the angle α approaches a value of $\pi/2$, indicating pure tensile failure mode⁸ rather than sliding failure of the two rigid blocks along the diagonal failure surface. The normalized depth h_0/h_{ef} of failure zone is also independent on h_{ef} when $d_B/h_{ef} = 0$, but reduced for higher d_B/h_{ef} .

Simple expressions for the angle α and the depth of the bottom failure zone h_0 may be obtained by regression analysis of the curves presented in Fig. 6. Nielsen concluded that the coefficient of friction μ_f for concrete can be identified as 0.75 by comparing test results of concrete with the rupture criteria for a modified Coulomb material. As $\mu_f = \tan \varphi$, the friction angle φ for concrete in a modified Coulomb material can be assumed to be 37° . Hence, the angle α can be represented by the following simple expression as an approximate solution of Eq. (12).

$$\alpha = 16.2(\mu)^{-0.15} + 37 \quad (13)$$

On the other hand, h_0/h_{ef} is also dependent on μ and d_B/h_{ef} as shown in Fig. 6, indicating that h_0/h_{ef} increases with the increase of μ and the decrease of d_B/h_{ef} . Although, h_0 could be calculated from Eq. (11), for most practical applications, h_0 would be simply expressed by non-linear regression analysis as follows:

$$h_0 = \left[0.9(\mu)^{0.06} - 0.21 \left(\frac{d_B}{h_f} \right) \right] h_f \quad (14)$$

Effectiveness factor of concrete

In the upper bound analysis above, concrete is regarded as perfectly plastic material. However, concrete, which is a typical brittle material, has a limited ductility in compression, and exhibits steep strain softening in tension. To correct for this and other shortcomings of applying the plasticity theory, an effectiveness factor of concrete is introduced. Different formulae^{7-9, 11, 12} based on

concrete properties, member geometry and loading condition have been proposed for the effectiveness factor of concrete in compression. In the present analysis, both concrete properties and size effect are represented in the expression for the compressive effectiveness factor of concrete.

Exner¹² showed that the plastic coefficient ν_p for concrete compressive strength can be determined from equating the area of the rigid-perfectly plastic stress-strain curve to that of the actual stress-strain curve of concrete. The plastic compressive coefficient commonly decreases with the increase of concrete compressive strength as a steeper slope of the descending part of the stress-strain curve of concrete develops in higher strength concrete.

From the statistical analysis of cylindrical specimens having concrete compressive strength less than 50 MPa (7250 psi), Roikjær et al.¹² suggested a value for the plastic compressive coefficient as follows:

$$\nu_p = \frac{3.2}{\sqrt{f'_c}} \quad (15)$$

Ductility of concrete is also strongly affected by specimen size. Eligehausen et al.^{13, 14} pointed out that the strain gradient at concrete breakout failure planes increases with the increase of h_{ef} , indicating that the nominal stress at failure decreases in proportion to $1/\sqrt{h_{ef}}$. ACI 318-05 also recommends that concrete breakout capacity of anchors should be modified by a size effect factor. Using the non-linear fracture mechanics, Bažant and Planas¹⁵ showed that the transverse tensile stress carrying capacity of concrete at diagonal crack surface decreases in proportion to $(1 + d/d_0)^{-1/2}$, where d = effective depth of concrete member and d_0 = coefficient defining the transition point between the strength criterion and linear elastic fracture mechanics. In the present study, Bažant and Kim's¹⁶ model below is employed to account for the size effect.

$$\nu_s = \frac{1}{\sqrt{1 + \frac{h_{ef}}{25d_a}}} \quad (16)$$

where d_a = maximum size of aggregate. The effectiveness factor ν_c of concrete compressive strength combining limited ductility of concrete and size effect can be expressed as follows:

$$\nu_c = \nu_p \nu_s = \frac{3.2/\sqrt{f'_c}}{\sqrt{1 + \frac{h_{ef}}{25d_a}}} \quad (17)$$

Much lower strength and ultimate strain as well as a steeper slope of the descending part of the stress-strain curve of concrete are observed in axial tensile tests than in axial compressive tests. It has been pointed out that it is so difficult to find an effectiveness factor ν_t of concrete tensile strength from purely tensile tests of concrete⁸. From the analytical model for punching shear of slabs, Nielsen⁸ suggested that the ratio μ of effective tensile strength to effective compressive strength of concrete would be in the range given below:

$$0.0025 \leq \mu = \frac{f_t^*}{f_c^*} \leq 0.01 \quad (18)$$

COMPARISONS AND DISCUSSIONS

Experimental data

The results of a large number of tests on different anchors in concrete subjected to tensile or shear load, carried out in both Europe and USA, were originally compiled by Fuchs et al.³ Other test results collected by Klingner et al.⁶ were added to the database. Additional test results for concrete strength above 50 MPa (7250 psi), carried out by Primavera et al.⁵, were also included to the database in the present study. To compare with predictions obtained from the mechanism analysis, the following criteria are considered in selecting specimens in the database: test specimens carried out in uncracked and unconfined concrete; single anchors subjected to short term tensile loads; specimens failing by concrete breakout and having no edge effect as specified in ACI 318-05. As a

result, the total number of specimens selected for the current investigation is 943: 501 specimens for cast-in-place anchors and 442 specimens for post-installed anchors.

The frequency distribution of main parameters influencing the concrete breakout capacity of selected anchors is presented in Fig. 7: Fig. 7(a) for concrete compressive strength and Fig. 7(b) for effective embedment depth of anchors. The test specimens were made of concrete having a very low compressive strength of 7.5 MPa (1087 psi) and a high compressive strength of 83 MPa (12035 psi), but concrete compressive strength less than 40 MPa (5800 psi) was dominant for most specimens. The effective embedment depth of cast-in-place and post-installed anchors ranged from 36 mm (1.14 in.) to 525 mm (20.7 in.) and from 18 mm (0.7 in.) to 203 mm (8.0 in.), respectively, indicating that a smaller effective embedment depth was employed in post-installed anchors than cast-in-place anchors. The majority of anchors in concrete specimens tested had an effective embedment depth below 125 mm (4.92 in.).

Comparison between predictions and test results

The concrete breakout capacities of anchors predicted by the iterative method (Eq. (9)) and simplified method (Eq. (10)) were reasonably close to each other as the difference in predictions was in a range between 3% and 7% for all anchors in the database. Therefore, the simplified mechanism analysis would be used for predicting concrete breakout capacity N_{cb} of anchors in the comparisons and parametric study given below. Fig. 8 presents the influence of μ on the mean $\gamma_{cs,m}$ and standard deviation $\gamma_{cs,s}$ of the ratio γ_{cs} between predictions $(N_{cb})_{Pre.}$ obtained from the mechanism analysis and measured concrete breakout capacity $(N_{cb})_{Exp.}$ of anchors in the database. The maximum size of aggregate and diameter of anchor head are assumed to be 20 mm (0.79 in.) and $0.15h_{ef}$, respectively, if they are not measured and given in the database. Concrete breakout capacity of anchors predicted from the mechanism analysis responds sensitively to the variation of

μ as the angle α and h_0 are influenced by μ (see Fig. 6). In addition, the plastic analysis for punching shear in slabs¹⁷ that is similar to concrete breakout failure of anchors showed that realistic results can be obtained when $\mu = 0.0025$. The mean $\gamma_{cs,m}$ and standard deviation $\gamma_{cs,s}$ increase with the increase of μ . For the upper limit of $\mu = 0.01$ recommended by Nielsen⁸, $\gamma_{cs,m}$ and $\gamma_{cs,s}$ of total specimens are 1.0 and 0.29, respectively, whereas, for the lower limit of μ of 0.0025, $\gamma_{cs,m}$ and $\gamma_{cs,s}$ of total specimens are 0.88 and 0.26, respectively. Fig. 8 shows that predictions obtained from the mechanism analysis are in good agreement with test results when μ falls into the range given in Eq. (18).

Comparisons of predictions obtained from ACI 318-05 and the mechanism analysis using $\mu = 0.01$ and 0.0025, and the measured concrete breakout capacity of anchors in the database are shown in Fig. 9; different statistical parameters for these comparisons are also given in Table 1. ACI 318-05 conservatively estimates concrete breakout capacity of anchors, namely, $\gamma_{cs,m}$ and $\gamma_{cs,s}$ are 0.78 and 0.15, respectively, for cast-in-place anchors and 0.72 and 0.17, respectively, for post-installed anchors. On the other hand, predictions by the mechanism analysis were closer to the experimental results than ACI318-05. However, prediction obtained by the mechanism analysis using $\mu = 0.0025$ was more conservative than that using $\mu = 0.01$. Coefficient of variation $\gamma_{cs,v}$ for cast-in-place anchors is smaller in ACI 318-05 than the mechanism analysis, while is similar in both methods for post-installed anchors as shown in Table 1. Therefore, the simplified procedure developed would be practically useful to predict the concrete breakout capacity of single anchors and failure planes overcoming the limitation of ACI 318-05 provisions mentioned earlier. However, it is more suitable for computer programming.

Effect of concrete compressive strength

The influence of concrete compressive strength f'_c on concrete breakout capacity N_{cb} of anchors is plotted in Fig. 10 using test results, and predictions by ACI 318-05 and the mechanism analysis using $\mu = 0.0025$. The concrete breakout capacity N_{cb} of anchors increases with the increase of f'_c ; however, the increasing rate is influenced by the effective embedment depth h_{ef} of anchors, agreeing with the neural network trained for estimating concrete breakout capacity of anchors under tension by Ashour and Alqedra¹⁸. For the cast-in-place anchors having h_{ef} above 200 mm (7.87 in.), predictions obtained from ACI 318-05 is more conservative than the mechanism analysis. For the post-installed anchors, ACI 318-05 predictions are highly conservative in specimens having concrete strength above 50 MPa (7250 psi), while the mechanism analysis shows better agreement with test results, regardless of concrete strength.

The internal energy dissipated in concrete is significantly dependent on the plastic compressive strength of concrete. The plastic compressive coefficient given by Eq. (15) is an empirical model based on the compressive cylinder tests having concrete strength below 50 MPa (7250 psi). This would be the main reason for the slight overestimation of N_{cb} for specimens having concrete strength above 50 MPa (7250 psi). Therefore, to conservatively predict N_{cb} in high-strength concrete, a lower plastic compressive coefficient of concrete, for example, $2/\sqrt{f'_c}$ which is the lower limit proposed by Nielsen⁸, would be used.

Effect of effective embedment depth of anchor

Fig. 11 shows the influence of effective embedment depth h_{ef} on the concrete breakout capacity N_{cb} of anchors. The concrete breakout capacity of anchors increases with the increase of h_{ef} . A higher increasing rate of N_{cb} against h_{ef} exhibited by cast-in-place anchors installed in high-strength concrete than concrete having strength below 40 MPa (1016 psi). Conservatism of ACI

318-05 increases with the increase of h_{ef} , in particular, cast-in-place anchors having $h_{ef} > 200\text{mm}$ (7.87 in.) and post installed anchors having $h_{ef} > 80\text{mm}$ (3.15 in.), whereas the mechanism analysis reasonably predicts test results. This indicates that the size effect given by Eq. (16) is successfully represented in the effectiveness factor.

Effect of anchor head diameter

The influence of the normalized diameter of anchor head d_B / h_{ef} on the concrete breakout capacity of cast-in-place anchors is presented in Fig. 12. The concrete breakout capacity of cast-in-place anchors slightly increases with the increase of d_B / h_{ef} as pointed out by Primavera et al⁵. The influence of the anchor head diameter on concrete breakout capacity and horizontal extent of failure planes in concrete surface is not considered in ACI 318-05, but properly reflected in the mechanism analysis as shown in Fig. 4 and Fig. 12.

CONCLUSIONS

A mechanism analysis based on upper-bound theorem is developed to predict the optimum failure surface generatrix and concrete breakout capacity of single anchors under tensile loads. The effect of different parameters on the concrete breakout capacity of anchors is also investigated. Comparison of extensive test results and predictions obtained from ACI 318-05 and the developed mechanism analysis are carried out. The following conclusions may be drawn:

1. The shape of failure surface generatrix predicted by the mechanism analysis is significantly influenced by the ratio of effective tensile and compressive strengths of concrete. For anchors installed in concrete having a ratio between effective tensile and compressive strengths of 0.0025, a much larger horizontal extent of failure planes in concrete surface is

predicted by the mechanism analysis than that recommended by ACI 318-05, agreeing with test results.

2. Concrete breakout capacity of anchors predicted from the mechanism analysis responds sensitively to the variation of the ratio between effective tensile and compressive strengths of concrete. Predictions obtained from the mechanism analysis are in better agreement with test results when the ratio between effective tensile and compressive strengths of concrete is 0.0025.
3. Conservatism of ACI 318-05 sharply increases in specimens having concrete strength above 50 MPa (7250 psi), while the mechanism analysis shows good agreement with test results, regardless of concrete strength.
4. A higher increasing rate of concrete breakout capacity of anchors against effective embedment depth is observed in high-strength concrete and cast-in-place anchors than in concrete having strength below 40 MPa (5800 psi) and post-installed anchors. For cast-in-place and post-installed anchors having effective embedment depth above 200 mm (7.87 in.) and 80 mm (3.15 in.), respectively, conservatism of ACI 318-05 dramatically increases with the increase of effective embedment depth of anchors, whereas predictions obtained from the mechanism analysis are in better agreement with test results.
5. Experimentally measured concrete breakout capacity of anchors slightly increases with the increase of the ratio of head diameter to effective embedment depth of anchors unlike ACI 318-05 provisions that ignore the anchor head diameter. The mechanism analysis reasonably reflects the influence of head diameter on the concrete breakout capacity of anchors.

ACKNOWLEDGMENTS

The authors wish to express their gratitude for the financial support by the Regional Research Centers Program (Bio-housing Research Institute) sponsored by the Korean Ministry of Education & Human Resources Development.

NOTATION

A	= area of failure surface
d_1	= horizontal extent of failure planes in concrete surface
d_a	= maximum size of aggregate
d_B	= diameter of anchor head
f_c'	= concrete compressive strength
f_c^*	= effective compressive strength of concrete
f_t	= concrete tensile strength
f_t^*	= effective tensile strength of concrete
h_{ef}	= effective embedment depth of anchor
h_0	= depth of the bottom failure zone as shown in Fig. 5
N_{cb}	= concrete breakout capacity of single anchors under tensile loads
W_A	= dissipated energy per unit area
W_E	= external work done by applied load
W_I	= total internal energy dissipated in failure surface
α	= angle between the relative displacement and failure surface
γ_{cs}	= ratio of predicted to measured concrete breakout capacity of anchors
$\gamma_{cs,m}$	= mean of γ_{cs}
$\gamma_{cs,s}$	= standard deviation of γ_{cs}
$\gamma_{cs,v}$	= coefficient of variation of γ_{cs}
δ	= relative displacement vector
μ	= ratio between effective tensile and compressive strengths of concrete ($= f_t^* / f_c^*$)

v_c = effectiveness factor for concrete compressive strength

v_p = plastic coefficient of concrete compressive strength

v_s = coefficient for size effect

v_t = effectiveness factor for concrete tensile strength

φ = friction angle of concrete

REFERENCES

1. ACI Committee 349, Nuclear Safety Structures Code and Commentary, Manual of Concrete Practice ACI 349, American Concrete Institute, 1989.
2. ACI Committee 318: Building Code Requirements for Structural Concrete (ACI 318-05) and Commentary (ACI 318R-05). American Concrete Institute, 2005.
3. Fuchs, W., Eligehausen, R, and Breen, J. E., “Concrete Capacity Design (CCD) Approach for Fastening to Concrete,” ACI Structural Journal, V. 92, No. 1, 1995, pp. 73-94.
4. Cannon, R. W., “Discussion of ‘Concrete Capacity Design (CCD) Approach for Fastening to Concrete,’ by Eligehausen, F. W., and Breen, J. E.” ACI Structural Journal, V. 92, No. 6, 1995, pp. 787-791
5. Primavera, E. J., Pinelli, J. P., and Kalajian, E. H., “Tensile Behavior of Cast-in-Place and Undercut Anchors in High-Strength Concrete,” ACI Structural Journal, V. 94, No. 5, 1997, pp. 583-594.
6. Klingner, R. E., and Mendonca, J. A., “Tensile Capacity of Short Anchor Bolts and Welded Studs: A Literature Review,” ACI Journal, V. 79, No. 4, 1982, pp. 270-279.
7. Chen, W. F., *Plasticity in Reinforced Concrete*, McGraw-Hill, New York, 1982.
8. Nielsen M. P. *Limit Analysis and Concrete Plasticity*, Prentice-Hall, Englewood Cliffs, 1984.
9. Bræstrup, M. W., “Punching Shear in Concrete Slabs,” *Plasticity in Reinforced Concrete*, Introductory Report, Colloquium of International Association for Bridge and Structural Engineering, Copenhagen, 1979, pp. 115-136.
10. Chapman, S. J., *MATLAB Programming for Engineers*, Thomson, USA, 2004.
11. Ashour, A. F., and Morley, C. T., “Effectiveness Factor of Concrete in Continuous Deep Beams,” *Journal of Structural Engineering*, ASCE, V. 122, No. 2, 1996, pp. 169-178.

12. Exner, H., Theory of Plasticity for Coulomb Materials, Ph. D. thesis, Technical University of Denmark, Denmark, 1983.
13. Eligehausen, R., and Ozbolt, J., "Size Effect in Anchorage Behaviour," Proceedings, European conference on Fracture Mechanics, Fracture Behaviour and Design of Materials and Structures, Turin, Oct. 1991, pp. 17-44.
14. Eligehausen, R., Bouska, P., Cervenka, V., and Pukl, R., "Size Effect on the Concrete Failure Load of Anchor Bolts," Fracture Mechanics of Concrete Structures, Elsevier Applied Science, 1992, pp. 517-525.
15. Bazant Z. P., and Planas J., *Fracture and Size Effect in Concrete and Other Quasibrittle Materials*. CRC Press, 1998.
16. Bažant Z. P., and Kim J. K., "Size Effect in Shear Failure of Longitudinally Reinforced Beams," ACI Journal, V. 81, No. 5, 1984, pp.456-468.
17. Bræstrup, M. W., Nielsen, M. P., Jensen, B. C., and Bach, F. "Axisymmetric Punching of Plain and Reinforced Concrete," Copenhagen, Technical university of Denmark, Structural Research Laboratory, Report No. R-75, 1976, 33 pp.
18. Ashour, A. F., and Alqedra, M. A., "Concrete Breakout Strength of Single Anchors in Tension using Neural Networks," Advances in Engineering Software, V. 36, 2005, pp. 87-97.

TABLES AND FIGURES

List of Tables:

Table 1 – Statistical comparison of $(N_{cb})_{pre.} / (N_{cb})_{Exp.}$ by different methods

List of Figures:

Fig. 1 – Concrete breakout failure mode idealized in ACI 318-05.

Fig. 2 – Axisymmetric failure surfaces divided into n segments.

Fig. 3 – Yield condition for a modified Coulomb material in plane strain.

Fig. 4 – Failure surface generatrices predicted by mechanism analysis.

Fig. 5 – Failure surface idealized by two straight generatrices.

Fig. 6 – Solution of α and h_0 / h_f against f_t^* / f_c^*

Fig. 7 – Frequency distribution of main parameters in the database

Fig. 8 – Effect of μ on $\gamma_{cs,m}$ and $\gamma_{cs,s}$.

Fig. 9 – Comparisons of predicted and measured N_{cb} .

Fig. 10 – Effect of f_c' on N_{cb} .

Fig. 11 – Effect of h_{ef} on N_{cb} .

Fig. 12 – Effect of d_B / h_{ef} on N_{cb} in cast-in-place anchors.

Table 1 – Statistical comparison of $(N_{cb})_{pre.} / (N_{cb})_{Exp.}$ by different methods

	ACI 318-05			Mechanism analysis					
	Cast-in-place	Post installed	All	$\mu = f_t^* / f_c^* = 0.01$			$\mu = f_t^* / f_c^* = 0.0025$		
				Cast in place	Post	All	Cast in place	Post installed	All
$\gamma_{cs,m}$	0.78	0.72	0.75	1.09	0.89	1.0	0.97	0.82	0.88
$\gamma_{cs,s}$	0.15	0.17	0.16	0.30	0.22	0.28	0.25	0.18	0.23
$\gamma_{cs,v}$	0.19	0.24	0.21	0.27	0.25	0.28	0.26	0.22	0.26

Note : $\gamma_{cs,m}$, $\gamma_{cs,s}$ and $\gamma_{cs,v}$ indicate the mean, standard deviation and coefficient of variation for the ratio of predicted and measured concrete breakout capacities, $\gamma_{cs} = (N_{cb})_{pre.} / (N_{cb})_{Exp.}$.

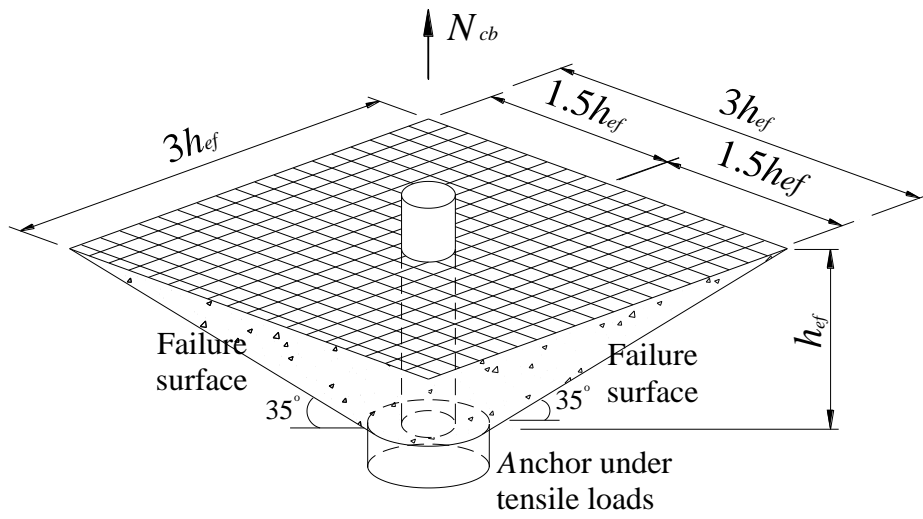


Fig. 1- Concrete breakout failure mode idealized in ACI 318-05.

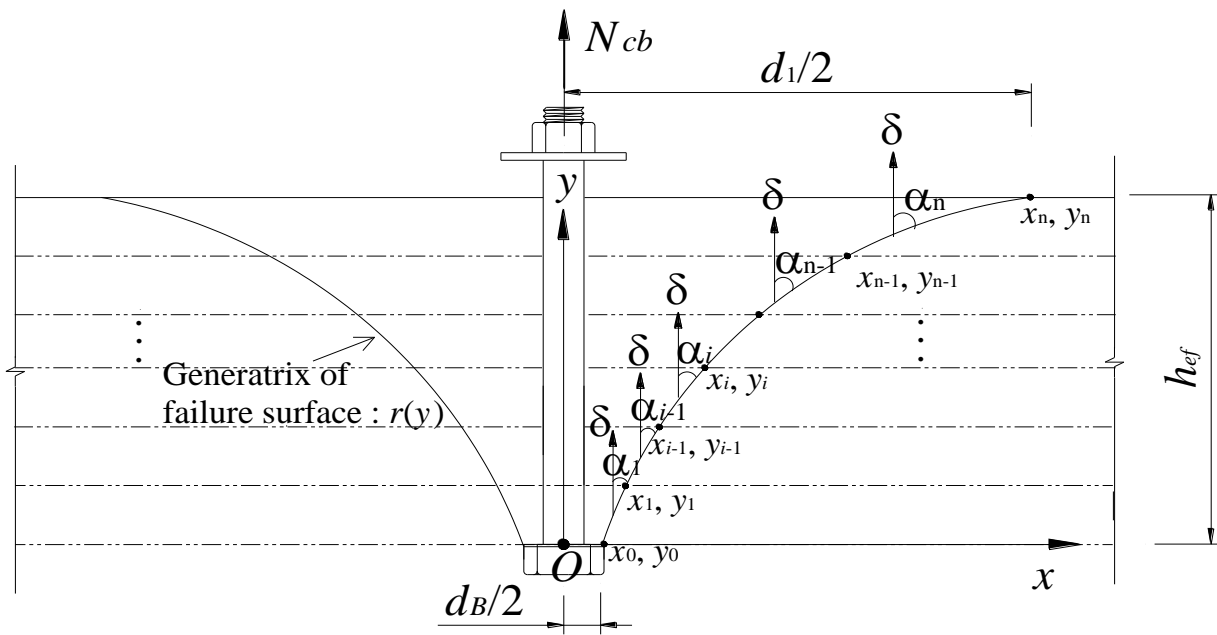


Fig. 2–Axisymmetric failure surfaces divided into n segments.

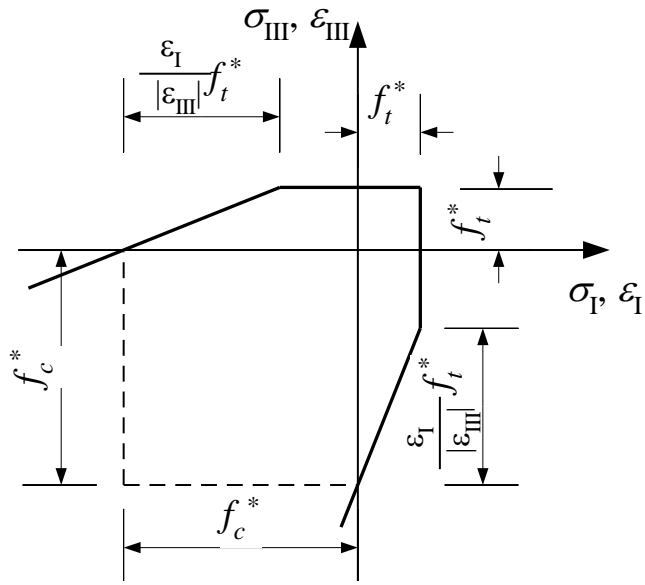
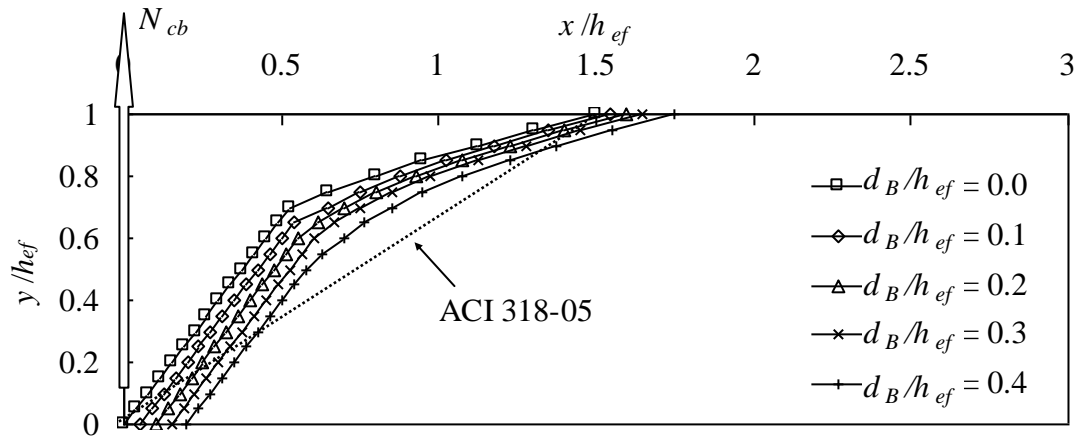
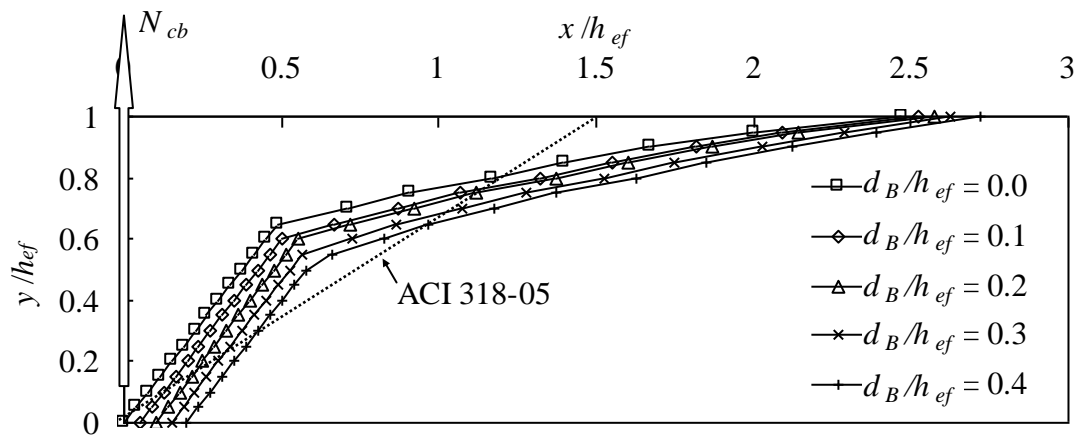


Fig. 3—Yield condition for a modified Coulomb material in plane strain.



(a) $\mu = f_t^* / f_c^* = 0.01$



(b) $\mu = f_t^* / f_c^* = 0.0025$

Fig. 4—Failure surface generatrices predicted by mechanism analysis.

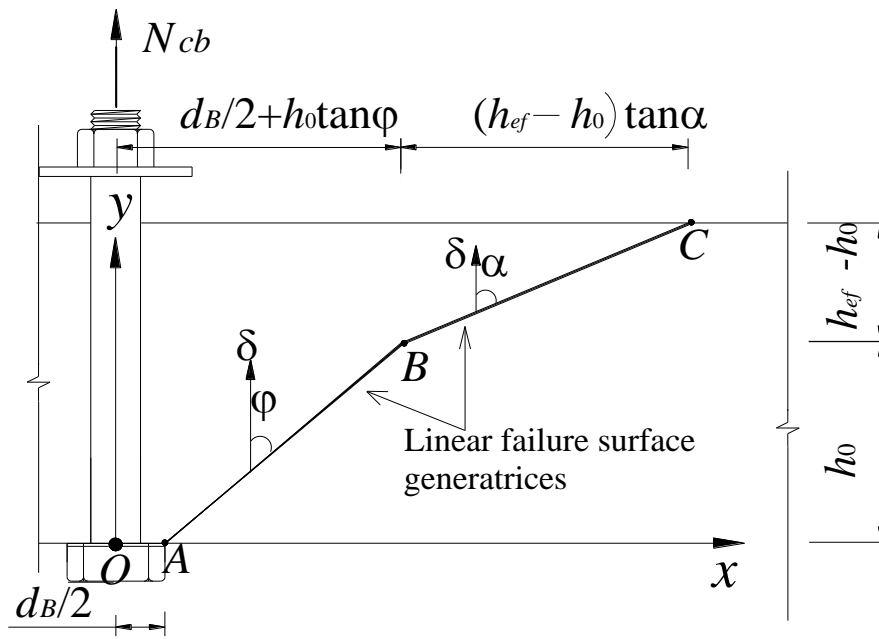


Fig. 5– Failure surface idealized by two straight generatrices.

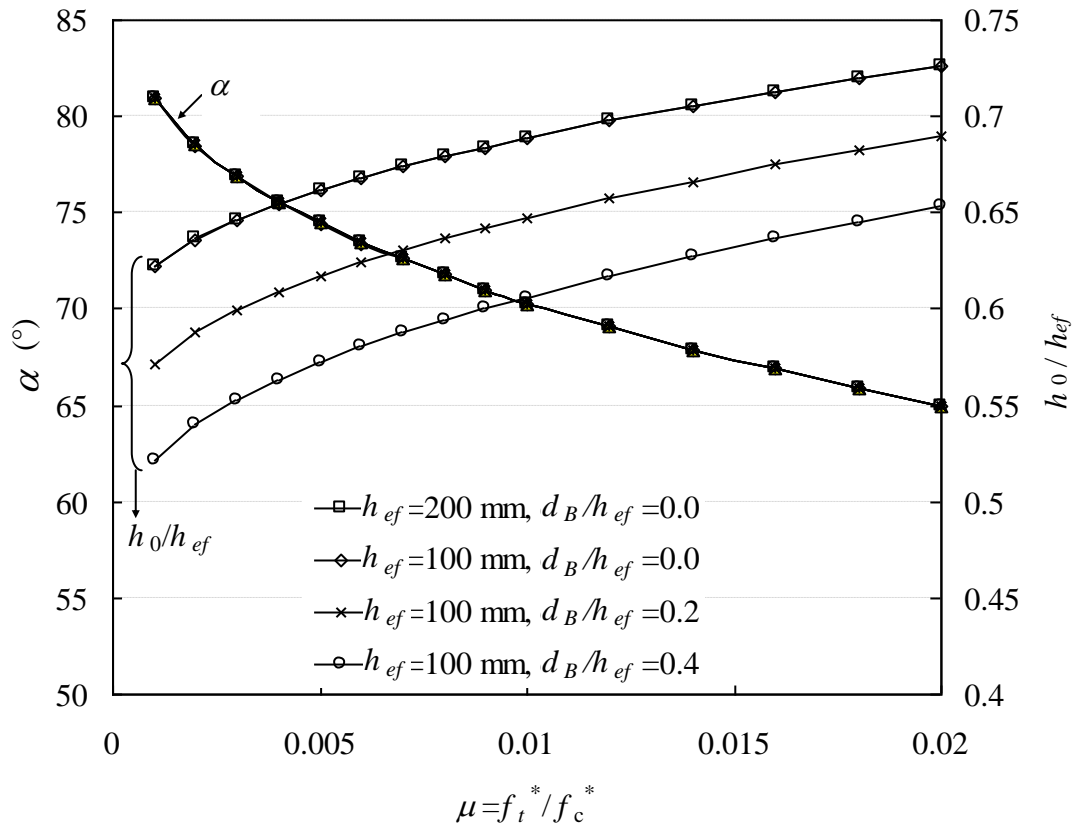
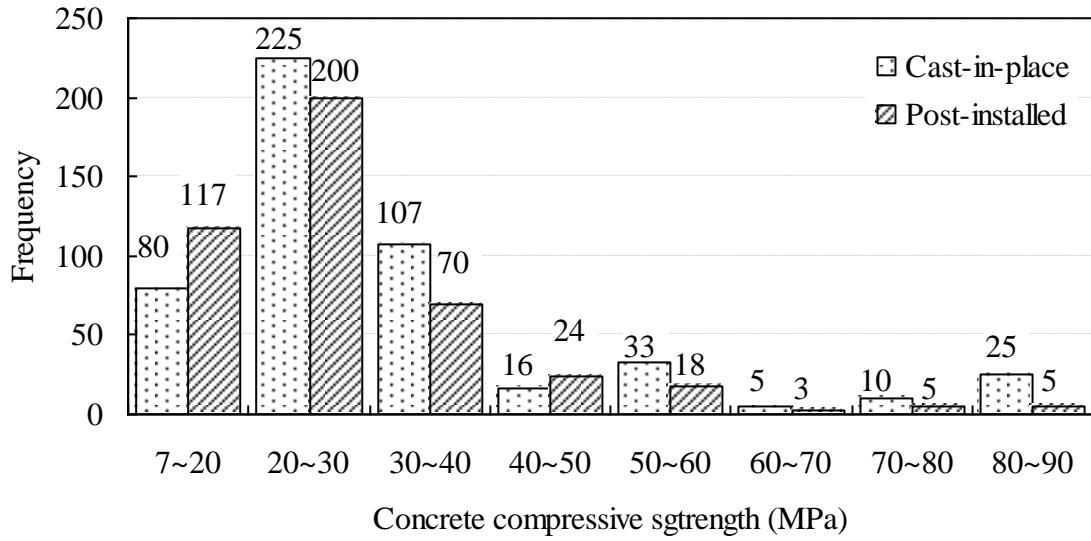
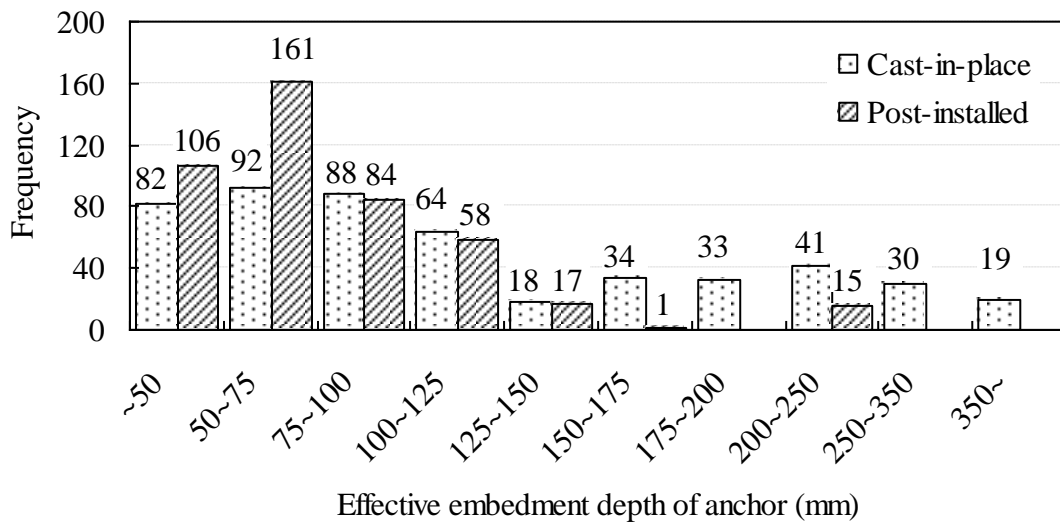


Fig. 6—Solution of α and h_0/h_{ef} against f_t^*/f_c^* (1 mm = 0.039 in.)



(a) Concrete compressive strength



(b) Effective embedment depth of anchor

Fig. 7–Frequency distribution of main parameters in the database

(1 MPa = 145 psi; 1 mm = 0.039 in.)

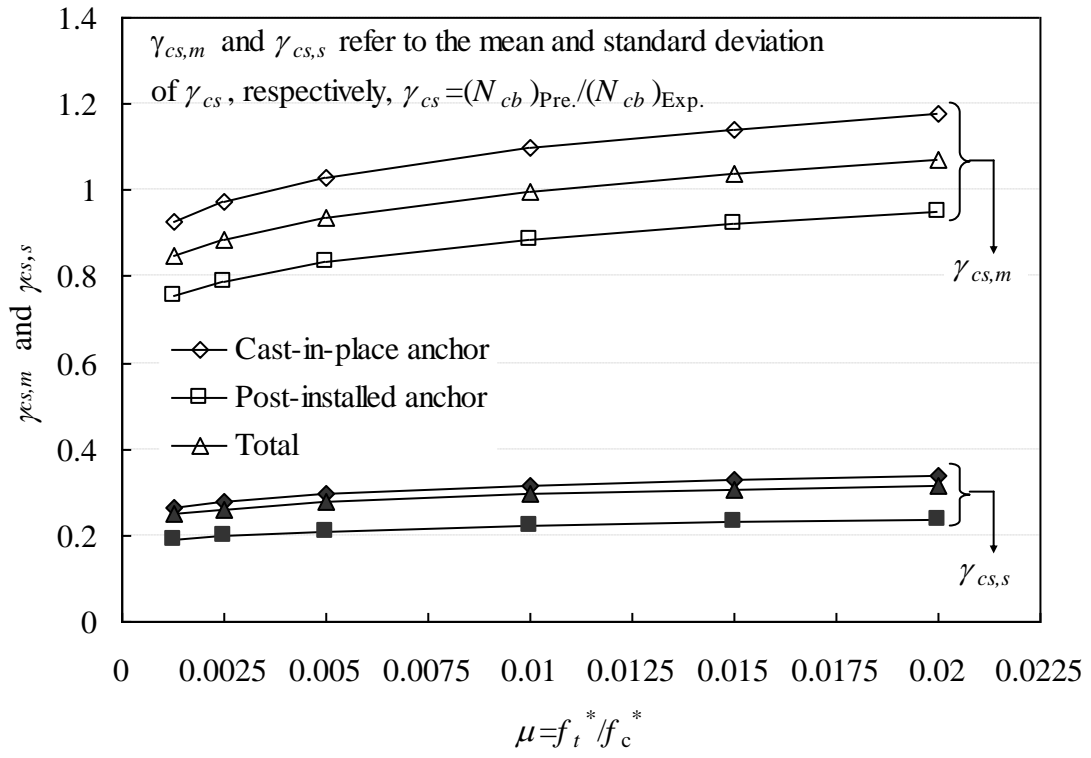
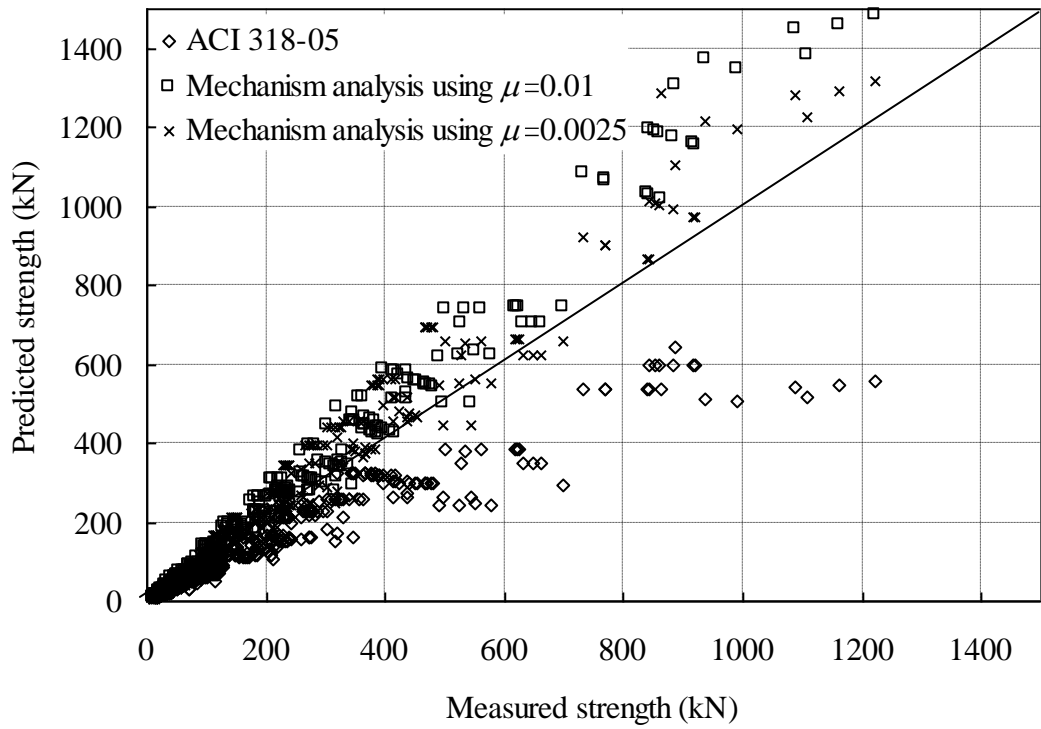
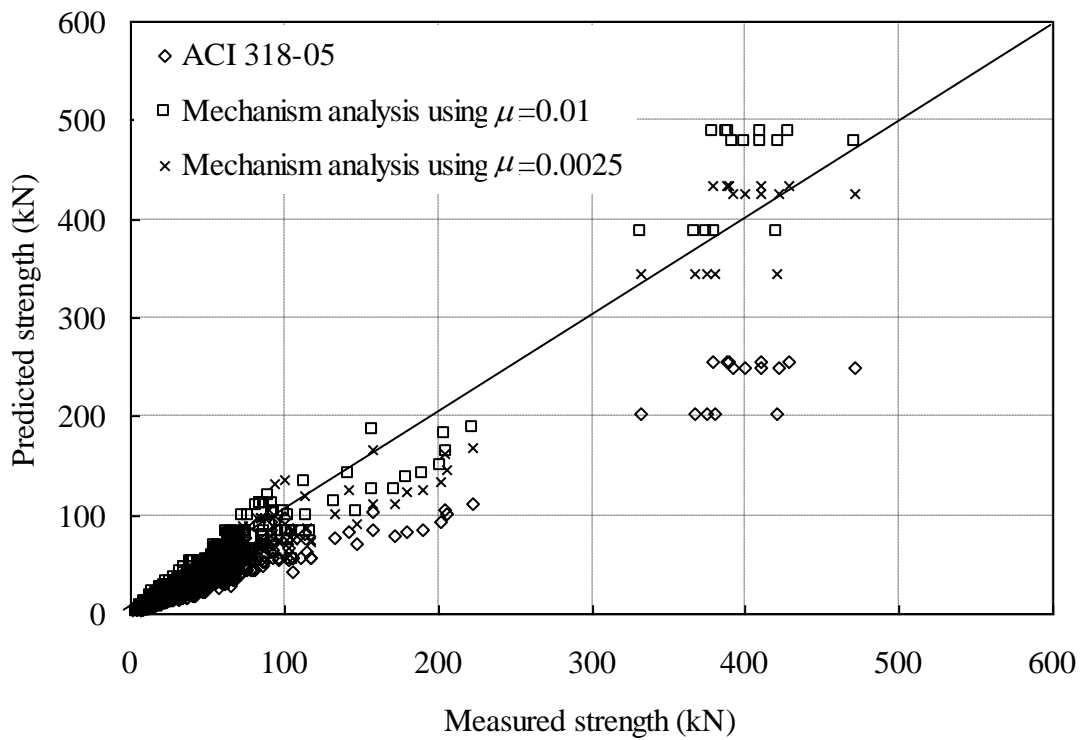


Fig. 8—Effect of μ on $\gamma_{cs,m}$ and $\gamma_{cs,s}$.

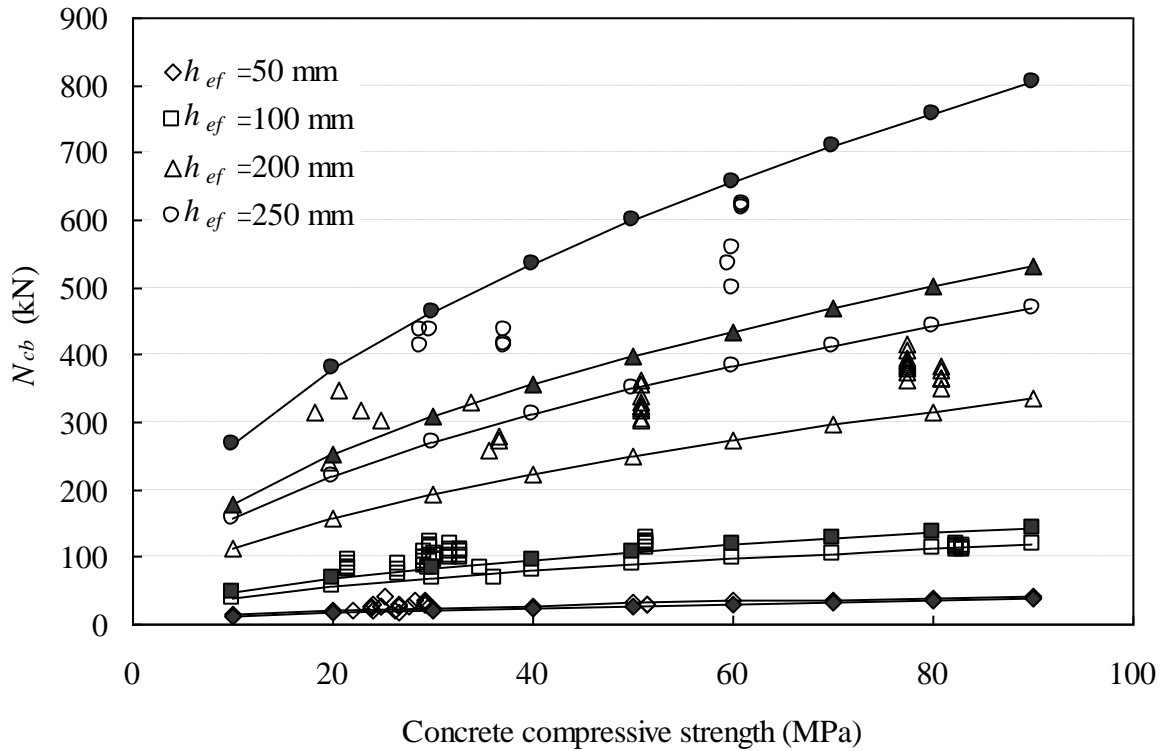


(a) Cast-in-place anchor

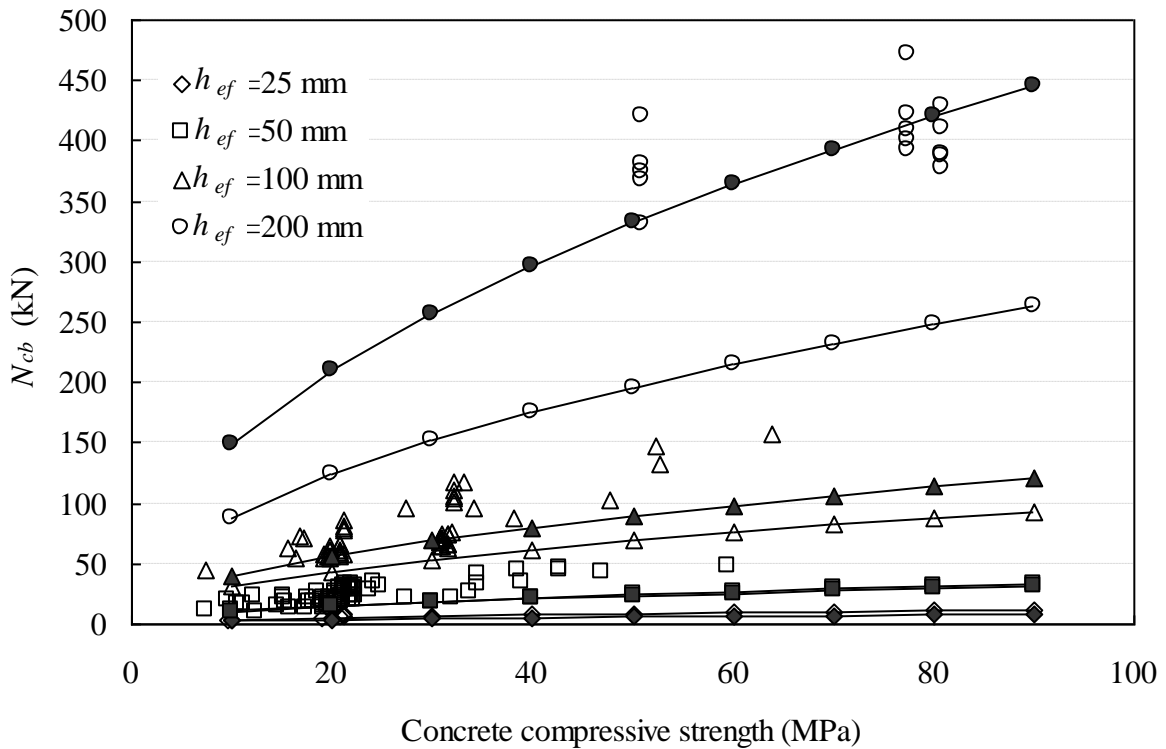


(b) Post-installed anchor

Fig. 9—Comparisons of predicted and measured N_{cb} . (1 kN = 0.2248 kips)

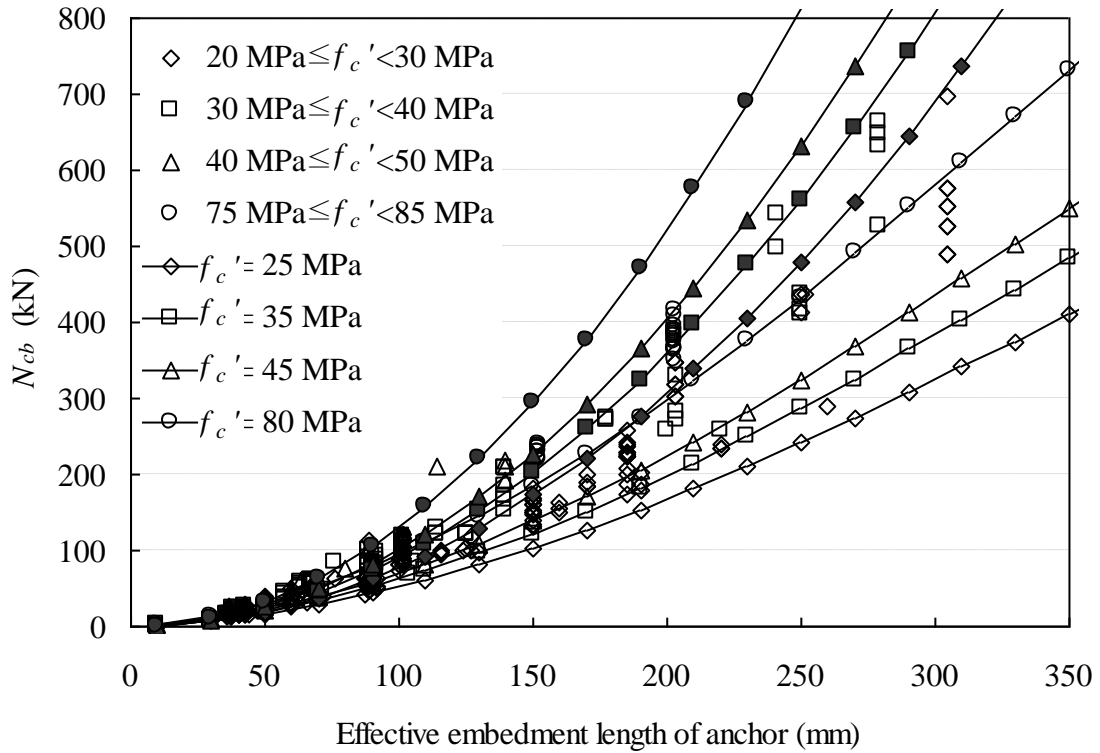


(a) Cast-in-place anchors

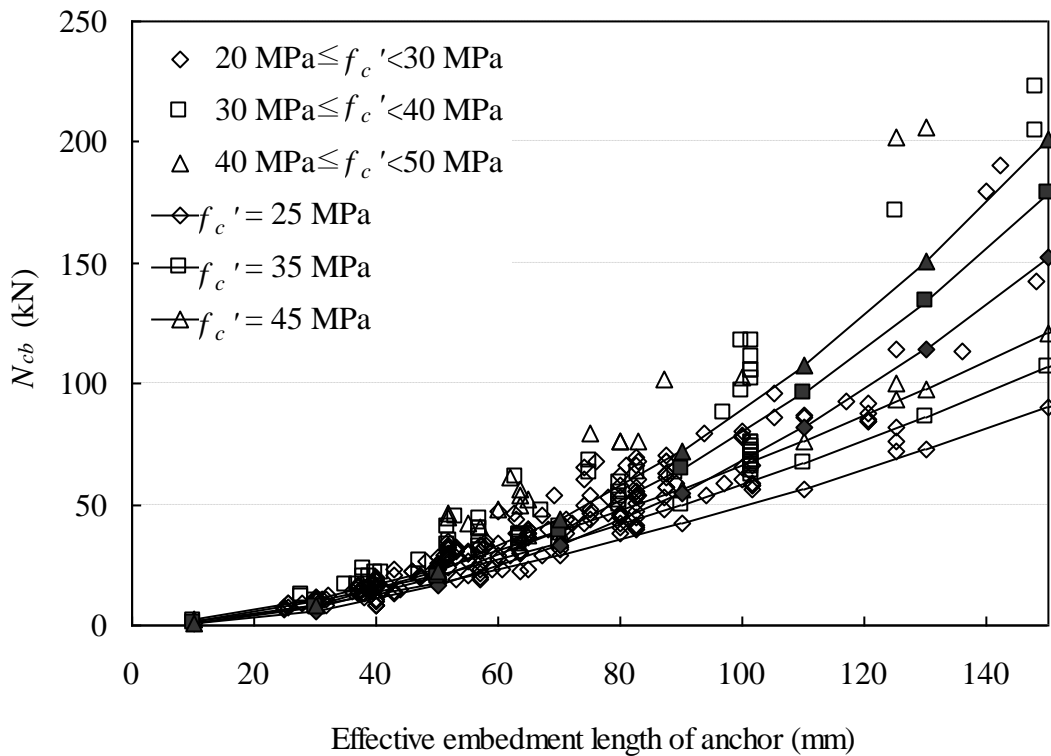


(b) Post-installed anchors

**Fig. 10—Effect of f'_c on N_{cb} . (1 MPa=145 psi; 1 kN=0.2248 kips; 1 mm=0.039 in.)
(Curves with white and black symbols indicate predictions by ACI 318-05 and mechanism analysis, respectively; whereas only white symbols indicate experimental results)**



(a) Cast-in-place anchors



(b) Post-installed anchors

**Fig. 11–Effect of h_{ef} on N_{cb} . (1 kN=0.2248 kips, 1 mm=0.039 in.; 1 MPa=145 psi)
(Curves with white and black symbols indicate predictions by ACI 318-05 and mechanism analysis, respectively; whereas only white symbols indicate experimental results)**

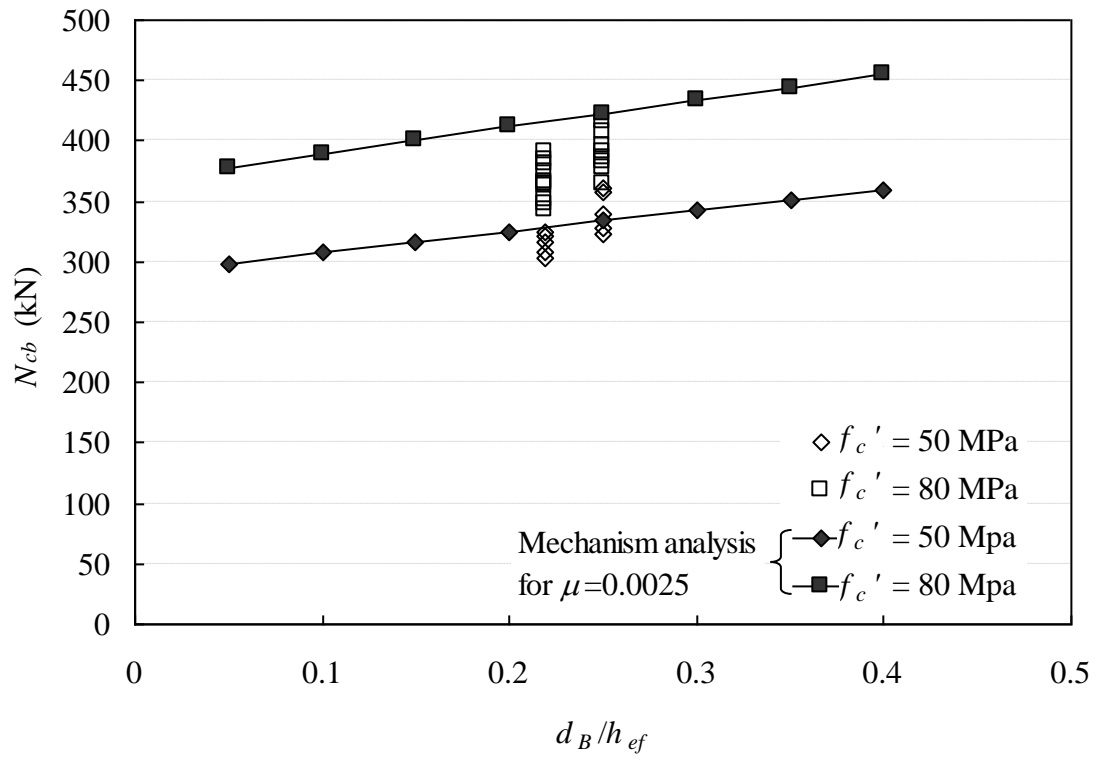


Fig. 12–Effect of d_B/h_{ef} on N_{cb} of cast-in-place anchors. (1 kN=0.2248 kips; 1 MPa=145 psi)
(Curves with black symbols indicate predictions by mechanism analysis; whereas only white symbols indicate experimental results)